Brittle strain regime transition in the Afar depression: Implications for fault growth and seafloor spreading

Anupma Gupta
Christopher H. Scholz
Lamont-Doherty Earth Observatory and Department of Earth and Environmental Sciences, Columbia University, Palisades, New York 10964, USA

ABSTRACT

Numerical and analogue models of fault-population evolution suggest that we should see a frequency-size transition from power law to exponential as brittle strain within a region increases. We now observe this transition in continental rift faults in the Afar region, Ethiopia and Djibouti. Furthermore, we observe that this strain transition is accompanied by a plateau in fault density and an increase in the displacement:length ratio of faults with increasing brittle strain. Once faults reach a critical density, stress shadows of nearby faults inhibit fault nucleation and restrict tip propagation. However, pinned faults continue to accommodate extension by accumulating more displacement, thus leading to higher displacement:length ratios in the higher strain regime. This strain regime transition is important to understanding the physics of fault growth and may also be important to rift localization and the development of plate boundaries.

Keywords: Afar, fault scaling, brittle strain, fault interaction.

INTRODUCTION

Observations of fault size, specifically displacement and length distributions, provide important constraints on physical models of fault growth as well as tests of model predictions. Numerical and clay models of fault-population evolution show that the size distribution of cracks has a transition from power law to exponential with increasing strain (Spyropoulos, 1999; Spyropoulos et al., 1999; Ackermann et al., 1997), and that crack density has a maximum value (Spyropoulos et al., 1999). Most observations of fault populations growing in low-strain regions show power law frequency-length scaling (Scholz and Cowie, 1990; Scholz et al., 1993; Scholz, 1997; Bohnenstiehl and Kleinrock, 1999). In higher strain settings, such as along the flanks of some mid-ocean ridges, faults have been observed to follow exponential frequency-size distributions (Cowie et al., 1993; Carbotte and Macdonald, 1994). Although Spyropoulos et al. (1999) suggested that these observations represent the end-member cases of their model observations, nowhere has this transition been observed in a single tectonic setting.

Another important scaling characteristic of fault populations is the linear relationship between fault displacement and length (Cowie and Scholz, 1992a; Dawers et al., 1993; Schlische et al., 1996). However, large variations in displacement:length ratios have been observed (Walsh and Watterson, 1988; Marrett and Allmendinger, 1991; Cowie and Scholz, 1992b; Gillespie et al., 1992). Much of the variation within similar tectonic settings has been attributed to fault interaction (Dawers and Anders, 1995; Cartwright et al., 1995; Wojtal, 1996; Willemse et al., 1996). Interaction can account for at least half the scatter in displacement:length ratios (Cartwright et al., 1995; Willemse et al., 1996; Gupta and Scholz, 2000). Poulimenos (2000) observed that higher displacement:length ratios correlate with high brittle strain regions in the Western Corinth graben, Greece. He is the first to link increasing strain to changes in displacement:length ratios. We see that for faults from the Afar triangle, not only are displacement:length ratios related to strain, but changes in fault size distribution, displacement:length ratios, fault density, and brittle strain are all intimately related to one another.

GEOLOGIC SETTING

The triple junction between the Arabian, Nubian, and Somalian plates is shown in Figure 1 (inset). Motion is accommodated by the East African Rift, the Sheba Ridge, the Red Sea Ridge, and faults in the Afar triangle. The three major plate boundaries are in different stages of evolution. Around the Sheba Ridge in the Gulf of Aden clear magnetic anomalies are identified to 10 Ma, although spreading may have started earlier (Cochran, 1981). The Red Sea began spreading 4–5 Ma (Roeser, 1975; Searle and Ross,

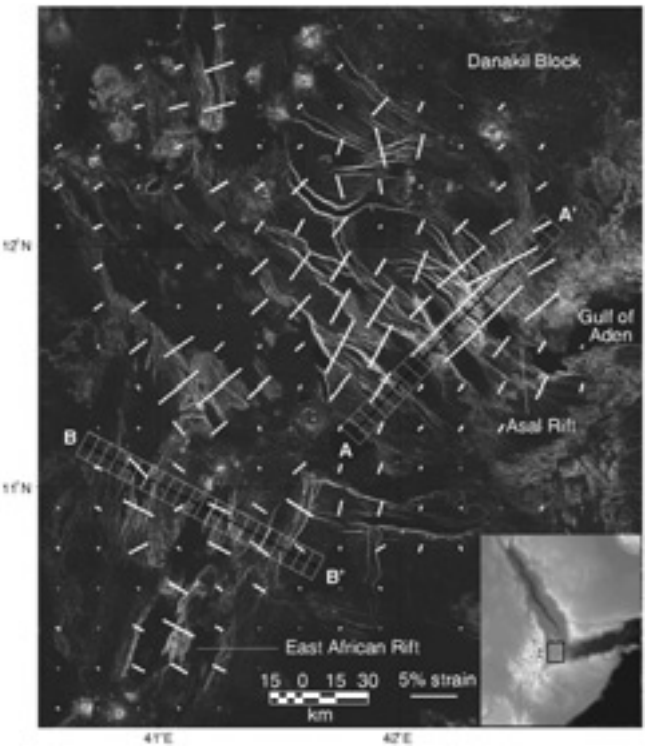

Figure 1. Location map and extension vectors. Inset shows extensional triple junction. Arabian plate is to north, Nubia is to west, and Somalia is to east. Area of larger image is outlined in inset. Larger image shows slopes calculated from digital elevation model and average extension vectors (thick white lines) for 18.5 × 18.5 km^2 regions. Maximum average extension for 342 km^2 regions is 9.0%. Steep slopes appear brighter. Linear features are faults. Circular features, such as those in northwest, are volcanoes. Fluvial channels are apparent on eastern edge of image. Transects mark locations of detailed fault-population analyses.

1975), while the East African Rift remains a continental rift.

The extended crust in the Afar triangle is influenced by all three plate boundaries as well as the Danakil block. The Danakil block is thought to have started as a piece of the Nubian plate and rotated counterclockwise 23° to its current position (Sichler, 1980; Collet et al., 2000). The relatively undeformed Danakil block forms the northern boundary of the Afar triangle. To the southwest and southeast, the Ethiopian Plateau looms 2 km above the floor of the Afar triangle. The plateau consists of Tertiary basalt formed through the influence of the Afar mantle plume (e.g., Mohr, 1983; Hofmann et al., 1997).

The nature of the crust in the Afar triangle is controversial (Makris and Ginsburg, 1987; Mohr, 1989). The crust is of intermediate thickness (15–25 km), and shows a velocity structure transitional between continental and oceanic (Berckhemen et al., 1975). The strength of the crust, measured as effective elastic thickness, decreases from 17 to 5 km in highly extended portions of Afar (Ebinger and Hayward, 1996). Much of the Afar triangle is covered in Pliocene basalt of the Stratoid series (Barberi and Varet, 1977). The northwest-southeast–trending Asal rift (Fig. 1) on the eastern edge of the Afar triangle is widely cited as a location where the beginnings of seafloor spreading can be observed on land (e.g., Stein et al., 1991).

We studied in detail the extension and fault-population characteristics across two transects. Faults that cross transect A–A′ are thought to be due to extension along the Arabia-Somalia plate boundary (Manighetti et al., 1998). However, the region just north of A′ belongs to the Danakil block, not Arabia (e.g., Collet et al., 2000). In any case, these faults are approximately perpendicular to the Arabia-Somalia motion vector (e.g., Jestin et al., 1994). The Asal rift (Fig. 1) is thought to accommodate most of the predicted present-day motion along this plate boundary (De Chabalier and Avouac, 1994). Faults that cross transect B–B′ clearly belong to the northernmost portion of the East African Rift, the boundary between the Nubian plate to the west and the Somalian plate to the east.

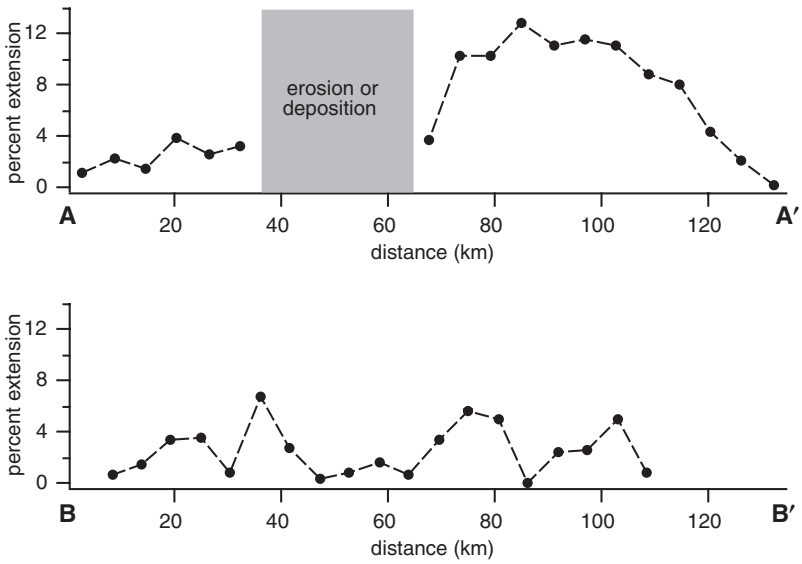

Figure 2. Average extension for 6 × 12 km² regions along A–A′ and B–B′ (indicated by white rectangles in Fig. 1). Maximum average extension is 12.9% for 72 km² subregions along A–A′ and B–B′. Assuming 30% increase in fault density with uniform offset of 10 m, estimated error in extension plots within symbol size.

STRAIN REGIME TRANSITION

Regional Extension

We measured extension for the area shown in Figure 1. Surface extension due to normal faults was measured using a 3 arcsecond digital elevation model of the region that provides 92 m horizontal and 10 m vertical resolution. Because the region has been recently resurfaced by volcanics, most of the high-frequency variability in the topography can be attributed to normal faulting. We calculated the vertical elevation difference between adjacent pixels. When this difference was not due to an obvious volcanic, fluvial, or erosional construct, we assumed that the elevation difference was created by normal faulting. Several weeks of field reconnaissance in the Asal rift confirmed the predominance of normal faulting. Observations of faults in the Asal rift indicate that they typically dip steeply, ~70°. Because faults may become steeper as they approach the surface, we assumed a crustal average fault dip of 60° for our calculation. Given fault throw and dip, we calculated the resulting heave or extension using simple trigonometry. Thus the extension estimates will vary with the cotangent of the fault dip. By assuming fault dip rather than using slopes calculated from the digital elevation model, we also minimized underestimation of fault dip due to undersampling or slumping. Changes in topography due to minor strike-slip motion, buried or eroded offset, deformation below data resolution, and low-frequency topographic variation are neglected in this analysis. Hence, the extension values presented in this study can be viewed as minimum values. We do not calculate the entire strain tensor.

Extension measured in the Afar triangle is shown in Figure 1. The thick white lines indicate the magnitude and direction of extension averaged in 18.5 km by 18.5 km regions. The extension averaged in this size region ranged from 0.0% to 9.0%. The primary features are the change in extension direction from northeast across the Asal rift to east-southeast across the East African Rift and the broad regions of strain localization centered on those rifts.

Detailed fault-population analysis was conducted along transects A–A′ and B–B′. Extension averaged in smaller subregions along these transects (indicated by white rectangles in Fig. 1) is shown in Figure 2. The zone of extension along both transects is about 100–120 km wide. In transect A–A′ maximum extensional strain within subregions is at about the 85 km point, just to the northwest of the Asal rift. Here it is believed that the beginning stages of slow seafloor spreading can be observed on land (Stein et al., 1991; De Chabalier and Avouac, 1994; Manighetti et al., 1998). We measure total brittle extension across transect A–A′ to be 8.5 km. In contrast, the extension across the East African Rift, transect B–B′, is diffuse and there is not one well defined extensional peak. The total extension across this transect, where seafloor spreading is not yet imminent, is 3.4 km.

Fault Scaling

Displacement length profiles for normal faults that are partially or fully contained within subregions shown in Figure 1 were extracted from the digital elevation model. Transects along the hanging wall were subtracted from profiles along the footwall to obtain displacement and length information. Fault density is calculated as fault length per unit area (km/km²) (Fig. 3). We estimate that fault lengths may be underestimated by 0.4–4.0 km, depending on the displacement gradients near tips. Lengths are underestimated because we lose resolution below 10–15 m of vertical offset. The error will be more significant for small faults because the missing length will represent a larger fraction of their total length. We have added a constant value of 2 km to fault lengths in Figure 4 to help account for the missing length (assuming that vertical offset below 12 m is not observed, and an observed displacement gradient of 0.012 near the tips).

We found that the fault density and displacement:length ratios change with the estimated brittle strain. At first the fault density increases ap-

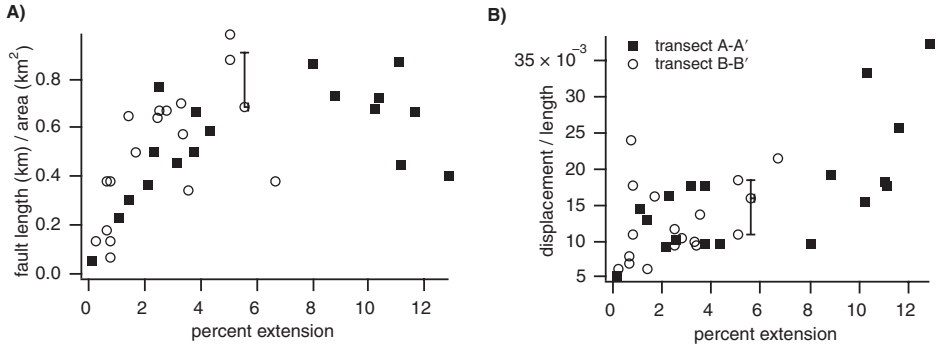

Figure 3. A: Fault density (kilometers of fault length per unit area) as function of estimated strain. Example error bar shows effect of 16 km of additional fault length with 10 m uniform offset. Extension estimate does not change significantly. B: Average displacement:length ratios for faults that are entirely or partially contained within subregions along transects plotted against percent extension. Example error bar shows uncertainty in displacement:length ratios and percent extension due to digital elevation model resolution. It is more likely that displacement:length ratios are slightly overestimated than underestimated because maximum offsets are accurate to within 10 m, but fault length could be underestimated by 0.4–4 km.

proximately linearly with strain, but at ~6%–8% the density levels off and does not increase further (Fig. 3A). Note that until about 8% extension, the displacement:length ratio remains relatively constant around 0.012 (Fig. 3B). Beyond 8% strain displacement:length ratios rise sharply from a mean value of 0.012 to 0.024. Brittle strain, ε, is proportional to *LWD,* where the width *W* is a constant width, *L* is fault length, and *D* is displacement. In the low-strain regime strain accumulates with increasing fault density (total fault length), whereas in the high-strain regime strain accumulates because of increased displacement on preexisting faults.

We also observe an evolution in the fault-population statistics (Fig. 4). The faults in subregions that accommodate <8% extension (filled circles) exhibit close to a power law frequency length distribution above the resolution cutoff at 4–5 km (Fig. 4A). In contrast, the fault size distribution in subregions that accommodate >8% extension (squares) is closer to an exponential (Fig. 4B). The maximum displacement distribution (not shown) exhibits the same basic relationships as the fault length distribution. Faults in low-extension subregions show power law scaling and faults in high-extension subregions show exponential scaling.

INTERPRETATION

Results show that brittle strain initially accumulates as a result of steady increase in fault density, but that the rate of increase in fault density with strain gradually diminishes until it reaches a steady-state value at 6%–8% strain, beyond which further strain is produced by increasing displacement:length ratios. The fault size distribution is power law in the low-strain regime but becomes exponential at high strain. Higher strain regions have relatively fewer small faults than regions with lower strain. These observations are the same as those observed by Spyropoulos et al. (1999) in a clay model. They interpreted these phenomena as resulting from an increase in fault interaction, nucleation of new faults being inhibited by stress shielding around preexisting faults and older faults being annihilated by coalescence (see also Ackermann and Schlische, 1997; Cowie, 1998). We have found, in addition, that high strains are accommodated by a progressive increase in the displacement:length ratio, which implies that, statistically, displacement is accommodated on faults that are no longer growing in length. This occurs because of pinning of fault growth by stress interaction with other faults (Gupta and Scholz, 2000; Contreras et al., 2000).

Poulimenos (2000) also observed higher displacement:length ratios in normal faults that occurred in higher strain settings in Greece. However, both high- and low-strain populations from the western Corinth graben showed power law frequency-length scaling. We favor Poulimenos' second interpretation for these observations. The faults in the higher strain region trend west-northwest and are crosscut by a population of smaller north-northeast–trending faults. These smaller faults serve to pin the west-northwest–trending fault population as stress fields do in Afar, preventing tip growth. The frequency-length distributions suggest that the west-northwest–trending faults from Greece have not entered a stage of growth dominated by coalescence.

CONCLUSIONS

We have observed fault populations in a single rock type and tectonic setting in different stages of evolution in the Afar triangle, a scenario previously only modeled. A strain regime transition from power law to exponential frequency-size scaling occurs when faults reach a certain density (about 0.6 km of fault length per square kilometer for the faults in Afar). Once this critical density is reached, little new fault surface area is created. Instead, faults must lengthen primarily by coalescence rather than by growth or nucleation. Saturation of fault surface area appears to occur as faults become pinned by the stress fields of

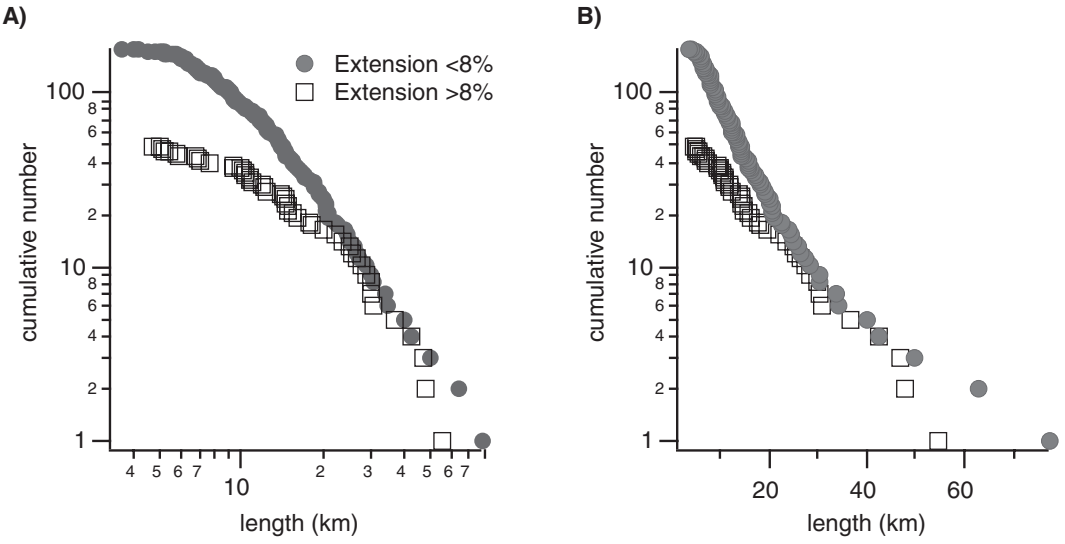

Figure 4. A: Cumulative number of faults vs. fault length, plotted on log-log axes. Cumulative number is calculated as number of faults with length greater than or equal to particular value. Power law relationships plot as straight line. B: As in A, except data are plotted on log-linear axes. Exponential relationships plot as straight line.

nearby faults. Their tips cannot easily propagate into stress shadows around nearby faults; new faults are also inhibited from nucleation by stress shadows. Displacement:length ratios must increase to balance stress shadows from nearby faults against stress concentrations near tips. In Afar, fault interaction plays a pivotal role in the strain transition.

ACKNOWLEDGMENTS

We thank J. Weissel for access to the digital elevation model and help with its analysis. We thank I. Manighetti and G. King for guidance with field work near the Asal rift. R. Bürgmann and R. Allmendinger provided constructive reviews. This research was supported by U.S. National Science Foundation grant EAR-9706475. Lamont-Doherty Earth Observatory contribution 6103.

REFERENCES CITED

Ackermann, R.V., and Schlische, R.W., 1997, Anticlustering of small normal faults around larger faults: Geology, v. 25, p. 1127–1130.

Ackermann, R.V., Schlische, R.W., and Withjack, M.O., 1997, Systematics of an evolving population of normal faults in scaled physical models: Geological Society of America Abstracts with Programs, v. 29, no. 6, p. A-198.

Barberi, F., and Varet, J., 1977, Volcanism of Afar: Small-scale plate tectonic implications: Geological Society of America Bulletin, v. 88, p. 1251–1266.

Berckhemen, H., Baier, B., Bartelsen, H., Behle, A., Burkhardt, H., Gebrande, H., Makris, J., Menzel, H., Miller, H., and Vees, R., 1975, Deep soundings in the Afar region and on the highland of Ethiopia, *in* Pilger, A., and Roesler, A., eds., Afar Depression of Ethiopia, Proceedings of an International Symposium on the Afar Region and Rift Related Problems, 1974: Stuttgart, Germany, E. Schweizerbart'sche Verlagsbuchhandlung, Volume 1, p. 89–107.

Bohnenstiehl, D.R., and Kleinrock, M.C., 1999, Faulting and fault scaling on the median valley floor of the trans-Atlantic geotraverse (TAG) segment, ~26°N on the Mid-Atlantic Ridge: Journal of Geophysical Research, v. 104, p. 29,351–29,364.

Carbotte, S.M., and Macdonald, K.C., 1994, Comparison of seafloor tectonic fabric at intermediate, fast, and super fast spreading ridges: Influence of spreading rate, plate motions, and ridge segmentation on fault patterns: Journal of Geophysical Research, v. 99, p. 13,609–13,631.

Cartwright, J.A., Trudgill, B.D., and Mansfield, C.S., 1995, Fault growth by segment linkage: An explanation for scatter in maximum displacement and trace length data from the Canyonlands grabens of SE Utah: Journal of Structural Geology, v. 17, p. 1319–1326.

Cochran, J.R., 1981, The Gulf of Aden: Structure and evolution of a young ocean basin and continental margin: Journal of Geophysical Research, v. 86, p. 263–287.

Collet, B., Taud, H., Parrot, J.F., Bonavia, F., and Chorowicz, J., 2000, A new kinematic approach for the Danakil block using a digital elevation model representation: Tectonophysics, v. 316, p. 343–357.

Contreras, J., Anders, M.H., and Scholz, C.H., 2000, Kinematics of normal fault growth and fault interaction in the central part of Lake Malawi Rift: Journal of Structural Geology, v. 22, p. 159–168.

Cowie, P.A., 1998, A healing-reloading feedback control on the growth rate of seismogenic faults: Journal of Structural Geology, v. 20, p. 1075–1087.

Cowie, P.A., and Scholz, C.H., 1992a, Physical explanation for the displacement length relationship of faults using a post-yield fracture mechanics model: Journal of Structural Geology, v. 14, p. 1133–1148.

Cowie, P.A., and Scholz, C.H., 1992b, Displacement to length scaling relationship for faults: Data synthesis and discussion: Journal of Structural Geology, v. 14, p. 1149–1156.

Cowie, P.A., Scholz, C.H., Edwards, M., and Malinverno, A., 1993, Fault strain and seismic coupling on mid-ocean ridges: Journal of Geophysical Research, v. 98, p. 17,911–17,920.

Dawers, N.H., and Anders, M.H., 1995, Displacement to length scaling and fault linkage: Journal of Structural Geology, v. 17, p. 607–614.

Dawers, N.H., Anders, M.H., and Scholz, C.H., 1993, Growth of normal faults: Displacement to length scaling: Geology, v. 21, p. 1107–1110.

De Chabalier, J.B., and Avouac, J.P., 1994, Kinematics of the Asal rift (Djibouti) determined from the deformation of the Fieale Volcano: Science, v. 265, p. 1677–1681.

Ebinger, C.J., and Hayward, N.J., 1996, Soft plates and hot spots: Views from Afar: Journal of Geophysical Research, v. 101, p. 21,859–21,876.

Gillespie, P.A., Walsh, J.J., and Watterson, J., 1992, Limitations of dimensions and displacement data from single faults and the consequences for data analysis and interpretation: Journal of Structural Geology, v. 14, p. 1157–1172.

Gupta, A., and Scholz, C.H., 2000, A model of normal fault interaction based on observations and theory: Journal of Structural Geology, v. 22, p. 865–879.

Hofmann, C., Courtillot, V., Féraud, G., Rochette, P., Yirgu, G., Ketefo, E., and Pik, R., 1997, Timing of the Ethiopian flood basalt event and implications for plume birth and global change: Nature, v. 389, p. 838–841.

Jestin, F., Huchon, P., and Gaulier, J.M., 1994, The Somalia plate and the East African Rift system: Present day kinematics: Geophysical Journal of the Interior, v. 116, p. 637–653.

Makris, J., and Ginzburg, A., 1987, The Afar Depression: Transition between continental rifting and sea-floor spreading: Tectonophysics, v. 141, p. 199–214.

Manighetti, I., Tapponnier, P., Gillot, P.Y., Jacques, E., Courtillot, V., Armijo, R., Ruegg, J.C., and King, G., 1998, Propagation of rifting along the Arabia-Somalia plate boundary into Afar: Journal of Geophysical Research, v. 103, p. 4947–4974.

Marrett, R., and Allmendinger, R.W., 1991, Estimates of strain due to brittle faulting: Sampling of fault populations: Journal of Structural Geology, v. 13, p. 735–738.

Mohr, P., 1983, Ethiopian flood basalt province: Nature, v. 303, p. 577–584.

Mohr, P., 1989, Nature of the crust under Afar: New igneous, not thinned continental: Tectonophysics, v. 167, p. 1–11.

Poulimenos, G., 2000, Scaling properties of normal fault populations in the western Corinth graben, Greece: Implications for fault growth in large strain settings: Journal of Structural Geology, v. 22, p. 307–322.

Roeser, H.A., 1975, A detailed magnetic survey of the southern Red Sea: Geologisches Jahrbuch, v. 13, p. 131–153.

Schlische, R.W., Young, S.S., Ackermann, R.V., and Gupta, A., 1996, Geometry and scaling relations of a population of very small rift-related normal faults: Geology, v. 24, p. 683–686.

Scholz, C.H., 1997, Earthquake and fault populations and the calculation of brittle strain: Geowissenschaften, v. 3-4, p. 124–130.

Scholz, C.H., and Cowie, P.A., 1990, Determination of total strain from faulting using slip measurements: Nature, v. 346, p. 837–838.

Scholz, C.H., Dawers, N.H., Yu, J.-Z., Anders, M.H., and Cowie, P.A., 1993, Fault growth and fault scaling laws: Preliminary results: Journal of Geophysical Research, v. 98, p. 21,951–21,961.

Searle, R.C., and Ross, D.A., 1975, A geophysical study of the Red Sea axial trough between 20.5° and 22°N: Royal Astronomical Society Geophysical Journal, v. 43, p. 555–572.

Sichler, B., 1980, La biellette danakile: Un modèle pour l'évolution géodynamique de l'Afar: Société Géologique de France, Bulletin, v. 22, p. 925–933.

Spyropoulos, C., 1999, A study of a complex system: Development of crack populations [Ph.D. thesis]: New York, Columbia University, 129 p.

Spyropoulos, C., Griffith, W.J., Scholz, C.H., and Shaw, B.E., 1999, Experimental evidence for different strain regimes of crack populations in a clay model: Geophysical Research Letters, v. 26, p. 1081–1084.

Stein, R.S., Briole, P., Ruegg, J.-C., Tapponier, P., and Gasse, F., 1991, Contemporary, Holocene, and Quaternary deformation of the Asal rift, Djibouti: Implications for the mechanics of slow spreading ridges: Journal of Geophysical Research, v. 96, p. 21,789–21,806.

Walsh, J.J., and Watterson, J., 1988, Analysis of the relationship between displacements and dimensions of faults: Journal of Structural Geology, v. 10, p. 239–247.

Willemse, E.J.M., Pollard, D.D., and Aydin, A., 1996, Three-dimensional analyses of slip distributions on normal fault arrays with consequences for fault scaling: Journal of Structural Geology, v. 18, p. 295–309.

Wojtal, S.F., 1996, Changes in fault displacement populations correlated to linkage between faults: Journal of Structural Geology, v. 18, p. 256–279.

Manuscript received May 1, 2000
Revised manuscript received August 28, 2000
Manuscript accepted September 8, 2000